Electronic structure of graphene twist stacks

S. Shallcross,[1,*] S. Sharma,[2] W. Landgraf,[1] and O. Pankratov[1]

[1]*Lehrstuhl für Theoretische Festkörperphysik, Staudstrasse 7-B2, D-91058 Erlangen, Germany*
[2]*Max Planck Institute for Microstructure Physics, Weinberg 2, D-06120 Halle, Germany*

We investigate the electronic structure of graphene stacks having an ordered sequence of pairs of twisted layers—the graphene twist stack. We find that this remarkable system entails a fundamental mixing of dimensionalities: While the twist stack spectrum is generated by an ensemble of independent effective twist bilayer Hamiltonians, the wave functions are products of bilayer wave functions and standing electron waves in the stacking direction, and thus extend over many layers of the stack. These have the property that of the ensemble of Dirac cones that constitute the twist stack band structure, it is those topologically closest to single layer graphene that dominate the surface region. We further examine the impact of stacking disorder, finding that these results are robust for moderate stacking fault density.

The practical realization of graphene via exfoliation in 2004[1] introduced a material of fundamental physical interest that, moreover, holds out the promise of profound technological innovation. However, hopes for progress toward a graphene based nanoelectronics lie not with exfoliated graphene flakes, which are limited in size to $\approx$100 μm, but with epitaxial graphene, which offers the possibility of a growth scalable up to macroscopic dimensions.[2–4] Among the most promising, both in terms of the quality of graphene epilayers as well as electron mobility, is that of graphene grown on the $(000\bar{1})$ face of SiC. Such growth results in a graphene stack that may consist of many epilayers (from tens to hundreds) that, crucially, have a largely ordered sequence of twisted layers. This is a fascinating material in its own right: a carbon allotrope that bridges the low-dimensional world of single layer graphene (SLG) Dirac-Weyl physics and the three-dimensional world of scalable epitaxial growth.

The impact of layer rotation upon the electronic properties of the graphene bilayer is now understood;[5–11] such rotation leads to an electronic decoupling in some energy window about the Dirac point (the width of which depends on the rotation angle) within which one finds degenerate SLG bands. Turning to the case of a graphene stack of $N_\perp$ layers a straightforward extension of this result would lead to the picture of a homogeneous system of decoupled layers, in that at any given layer a similarly decoupled graphene cone could, in principle, be accessed. In fact, as we show, the high degree of azimuthal stacking order found in this system dramatically alters this picture.

It turns out that for bilayer periodic twist stacks the Hamiltonian may be expressed as a set of independent effective bilayer Hamiltonians, each having an interlayer coupling scaled by $0 < \lambda < 2$. The twist stack spectrum is therefore simply a superposition of effective twist bilayer band structures and this system thus remains, in an essential way, a two-dimensional system irrespective of the number of layers in the stack. The extended nature of the twist stack is, however, manifest in the stack wave functions, which consist of a direct product of two-dimensional bilayer states with one-dimensional states that are standing electron waves in the stacking direction. These standing waves have a number

of universal characteristics leading in turn to certain universal characteristics of bilayer periodic twist stacks. In particular, we show that bands from large λ bilayers are, by these standing waves, confined to the interior of the stack. In contrast, low λ bands, topologically much closer to those of SLG, oscillate over the whole stack, and in particular may be accessed from the surface. The twist stack is thus a strikingly heterogeneous system.

To focus on the interlayer electronic motion we first imagine the stack to be composed of doubly periodic one-dimensional chains of atoms, as illustrated schematically in Fig. 1. A single chain thus contains one atom from each layer and, given that there are $N_\parallel$ sites per layer, this leads to $N_\parallel$ such chains. To make further progress we consider a realistic tight-binding scheme that consists of s, p_x, p_y, and p_z orbitals situated at every site of the stack. An arbitrary element of the tight-binding Hamiltonian H may then be labeled by a pair of chain, layer, and orbital indices. H may therefore be written in block matrix form with each block $H^{\alpha\beta}$ an $N_\perp \times N_\perp$ matrix whose individual elements describe electron hopping from an atomic orbital at layer i of chain α to another orbital at layer j of chain β. (Here and in the following we suppress implied orbital indices in $H^{\alpha\beta}$.)

We now introduce two key approximations: (i) electron hopping between nearest neighbor layers only and, (ii), decoupling of the sp^2- and π-band systems, both known to be excellent approximations for graphene stacks. The decoupling of the sp^2- and π-band systems evidently amounts to the neglect of p_z to non-p_z hopping integrals, the importance of which is that then all overlap integrals are then unchanged upon transforming the hopping vector from $\delta\mathbf{r} = (\delta x, \delta y, \delta z)$ to $\delta\mathbf{r} = (\delta x, \delta y, -\delta z)$. This leads to the form for $H^{\alpha\beta}$ shown in Fig. 1. By further adopting the symmetrized representation $t_{\perp\sigma}^{\alpha\beta} = (t_{\perp 1}^{\alpha\beta} + \sigma t_{\perp 2}^{\alpha\beta})/2$ ($\sigma = \pm 1$), and similar for $t_{\parallel\sigma}^{\alpha\beta}$, one finds that $H^{\alpha\beta}$ may be written in terms of elementary matrices as

$$H^{\alpha\beta} = \sum_\sigma \left(t_{\perp\sigma}^{\alpha\beta} \mathbf{I}_\sigma \cdot \mathbf{T} + t_{\parallel\sigma}^{\alpha\beta} \mathbf{I}_\sigma \right), \qquad (1)$$

where $\mathbf{I}_\sigma$ is a diagonal matrix with $[\mathbf{I}_\sigma]_{ii} = \sigma^{i+1}$ and $\mathbf{T}$ is a Toeplitz matrix defined as $T_{ii\pm1} = 1$ and all other elements
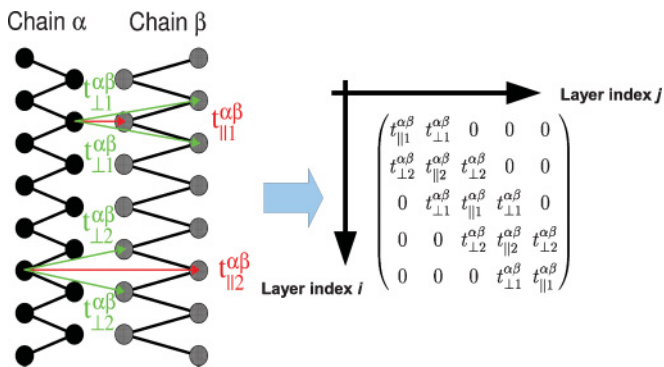
FIG. 1. (Color online) Schematic illustration of the grouping of graphene stack atoms into one-dimensional chains along with hopping processes that lead to the inter- ($t_{\perp i}^{\alpha\beta}$) and intralayer ($t_{\parallel i}^{\alpha\beta}$) matrix elements of $H^{\alpha\beta}$.

zero. The simplicity of form found in Eq. (1) suggests the use of basis functions for $H^{\alpha\beta}$ based on the eigenfunctions of **T** (an approach followed also in Ref. 12 which we here generalize). These eigenfunctions are standing waves in the azimuthal direction, with projection on the jth layer given by

$$\psi_m(j) = \frac{1}{\sqrt{N_\perp + 1}} \sin\left[\frac{-m + N_\perp + 1}{2(N_\perp + 1)}\pi j\right], \quad (2)$$

and corresponding eigenvalues $\lambda_m = 2\sin[m\pi/(2N_\perp + 2)]$ where $m = -(N_\perp - 1), -(N_\perp - 3), \ldots, (N_\perp - 1)$. Examples of such standing waves are displayed in the insets of Fig. 2 for the cases $m = 0$ and $m = 10$ ($N_\perp = 11$ in both cases). The appropriate basis for $H^{\alpha\beta}$ is then constructed from equal $|m|$ functions as $|\Phi_{m\sigma}\rangle = (|\psi_m\rangle + \sigma|\psi_{-m}\rangle)/\sqrt{2}$ ($m \neq 0$) where $\sigma = \pm 1$. For the case $m = 0$ we simply set $|\Phi_0\rangle = |\psi_0\rangle$. Using $\mathbf{T}|\psi_m\rangle = \lambda_m|\psi_m\rangle$ and the fact that $\mathbf{I}_\sigma|\psi_m\rangle = |\psi_{\sigma m}\rangle$, one immediately finds that $H^{\alpha\beta}$ is, in this basis, block diagonal in m with, for $m > 0$, each $\sigma\sigma'$ block being given by

$$[H^{\alpha\beta}]_{mm} = \begin{pmatrix} t_{\parallel 1}^{\alpha\beta} & \lambda_m t_{\perp 1}^{\alpha\beta} \\ \lambda_m t_{\perp 2}^{\alpha\beta} & t_{\parallel 2}^{\alpha\beta} \end{pmatrix}, \quad (3)$$

while for $m = 0$ we have $[H^{\alpha\beta}]_{00} = t_{\parallel 1}^{\alpha\beta}$. Note that σ space is clearly isomorphic to the layer space of the identical bilayer portions of the two chains. The fact that every block $H^{\alpha\beta}$ of the stack Hamiltonian may be treated in this way immediately implies that the full stack Hamiltonian may be similarly brought to block diagonal form in m as

$$H = \begin{cases} \bigoplus_{m=1}^{m=(N_\perp - 1)} H_{\text{bilayer}}(\lambda_m) & N_\perp \text{ even,} \\ \bigoplus_{m=2}^{m=(N_\perp - 1)} H_{\text{bilayer}}(\lambda_m) \oplus H_{\text{SLG}} & N_\perp \text{ odd,} \end{cases} \quad (4)$$

where $H_{\text{bilayer}}(\lambda_m)$ is an effective bilayer Hamiltonian, identical to the physical $N_\perp = 2$ bilayer Hamiltonian, but with all interlayer interactions scaled by λ_m, and H_{SLG} is the physical SLG Hamiltonian. Note that although $H^{\alpha\beta}$ is clearly not Hermitian, Hermiticity of the full Hamiltonian is ensured by $H^{\alpha\beta} = (H^{\beta\alpha})^\dagger$. As we have made no assumption concerning the in-plane unit cell in this derivation, which may be arbitrarily complex, we conclude that for a general two-periodic graphene stack we have a spectrum determined by the independent low-dimensional Hamiltonians $H_{\text{bilayer}}(\lambda_m)$ and H_{SLG}. A stack eigenstate is thus labeled by the usual band and k-vector labels,
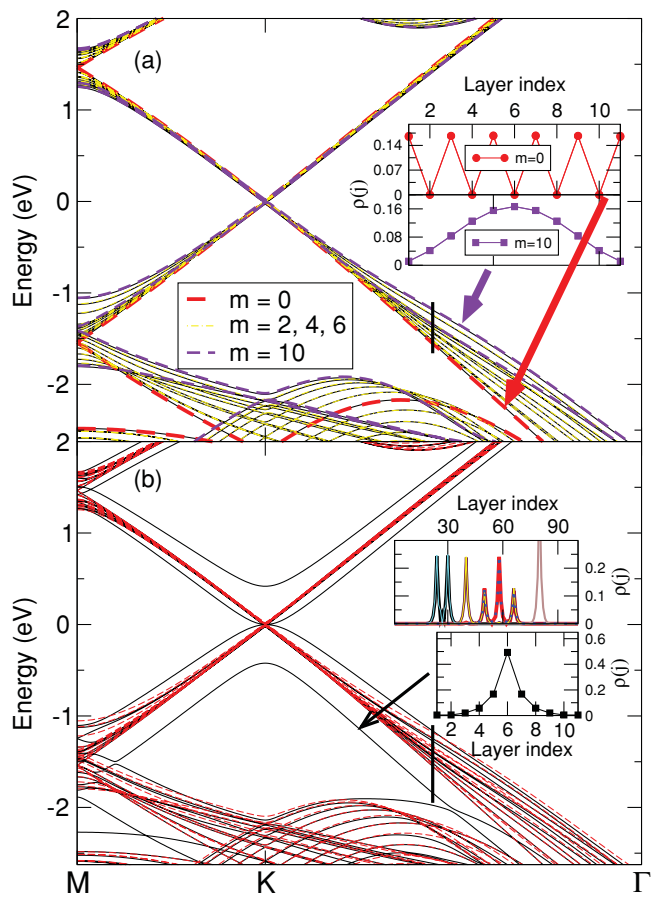

FIG. 2. (Color online) Band structure of an 11-layer twist stack ($\theta = 21.78°$) ideal system shown in (a) while in (b) a single rotation fault has been introduced. In both panels colored dashed lines indicate the band structure given by Eq. (4), with full black lines the directly calculated twist stack band structure. Insets in panel (a) show the layer-integrated density $\rho(j)$ for the stack states arising from bands indicated by arrows. Lower inset panel displays $\rho(j)$ of the defect states associated with the defect band indicated by arrow, with upper inset panel similar but for a 101-layer stack with seven randomly distributed twist faults. See text for details.

n and $\mathbf{k}$ respectively, but in addition the new standing wave *good* quantum number m.

A property of particular interest is the spatial distribution in the stacking direction of the eigenstates of Eq. (4); this will determine those states accessible at the surface of the twist stack and those confined to the interior. In this connection the key object is evidently the layer integrated probability density of each stack eigenstate, $\rho_{n\mathbf{k}}^{(m)}(j)$. The block diagonal structure in m of Eq. (4) ensures that after integrating out in-plane degrees of freedom, i.e., integrating out the chain index α, $\rho_{n\mathbf{k}}^{(m)}(j)$ will involve only pairs of standing waves with identical m, $\Phi_{m+}(j)$ and $\Phi_{m-}(j)$:

$$\rho_{n\mathbf{k}}^{(m)}(j) = \sum_\sigma c_{n\mathbf{k}}^{(m)}(\sigma)\Phi_{m\sigma}^2(j). \quad (5)$$

Here $c_{n\mathbf{k}}^{(m)}(\sigma)$ are coefficients that result from integrating over the chain degrees of freedom of the stack states. Given that $H_{\text{bilayer}}(\lambda_m)$ is the Hamiltonian of identical rotated graphene

layers, and that σ space is isomorphic to layer space, we must have $c_{n\mathbf{k}}^{(m)}(+1) = c_{n\mathbf{k}}^{(m)}(-1) = 1/2$. For this case the definition of $\Phi_{m\sigma}(j)$ and the fact that $\psi_m(j) = (-1)^j \psi_{-m}(j)$ then yield for the density profile $\rho(j) = \psi_m^2(j)$ which, as it depends only on the quantum number of the standing wave m, is universal for all graphene stacks. Furthermore, from Eq. (2) we see that this universal form has the property that the surface density $\psi_m^2(1)$ decreases as m increases, and thus that high m distorted Dirac cones will be confined to the interior of the stack.

To elucidate some of the consequences of this result for the graphene twist stack, and to investigate the validity of the approximations involved in deriving it, we now turn to numerical tight-binding (TB) calculations. Our TB parametrization follows the form proposed by Tang *et al.* in Ref. 13, with new graphene-specific hopping integrals obtained by optimizing the TB error over a data set of few-layer graphene stacks calculated *ab initio*.

We first consider, in panel (a) of Fig. 2, the band structure of an 11-layer twist stack in which every second layer is rotated by $\theta = 21.78°$. One immediately sees that the band structure given by Eq. (4) coincides precisely with that of a direct tight-binding calculation of the twist stack band structure, confirming that the spectrum of this system is indeed that of an ensemble of one- and two-layer Hamiltonians. In particular, there are bands coinciding exactly with those of SLG ($m = 0$) in addition to bands from strongly coupled effective bilayers ($m = 10$). For hole states these latter bands are, due to the increased coupling of the $m = 10$ effective bilayer ($\lambda = 1.93$), linear in a much reduced energy window as compared to SLG. Interestingly, this deviation from the SLG Dirac cone of the large m bands is strikingly asymmetric, being much reduced for electron states as compared to hole states, a result true for the physical twist *bilayer* [5,6,8] that thus transfers to the twist *stack*. A further instance of this transference which, it should be stressed, is due to fact that the twist stack spectrum is a superposition of effective twist bilayer spectrums, is that the SLG Dirac cone provides a lower (upper) bound on the $N_\perp$ hole (electron) Dirac cones.

We now return to the question of the accessibility at the surface of the stack of the various twist stack states. First, we note that the insets of Fig. 2, which display $\rho(j)$ for the $m = 0$ and $m = 10$ states, show the expected behavior, the latter state being entirely confined to the interior. To investigate this further we present, in Fig. 3, numerical values for the coefficients $c_{n\mathbf{k}}^{(m)}(\sigma)$ for various twist stack systems. As may be seen, for energies close to the SLG energy a transition occurs from the expected $c_{n\mathbf{k}}^{(m)}(+1) = c_{n\mathbf{k}}^{(m)}(-1) = 1/2$ to a case where these coefficients take instead the values [1,0] or [0,1]. This behavior, which we find for all systems studied,[14] results from the fact that as $\lambda \to 0$ the interlayer matrix elements become comparable to the matrix elements due to mixing of the sp^2- and π-band systems. The impact of this on the surface density is illustrated in Fig. 4 in which $\rho(1)$ is plotted for those states intersecting the black vertical line in Fig. 2, for both the 11-layer ($\theta = 21.78°$) system as well as an identical system but with 101-layers. As expected, as the eigenenergy moves away from that of SLG the $\rho(1)$ of the associated state drops to zero; however, as $E \to E_{SLG}$ the two branches of $\rho(1)$ meet before bifurcating into low and high surface density solutions. This arises from the transition in the $c_{n\mathbf{k}}^{(m)}(\sigma)$, which in turn
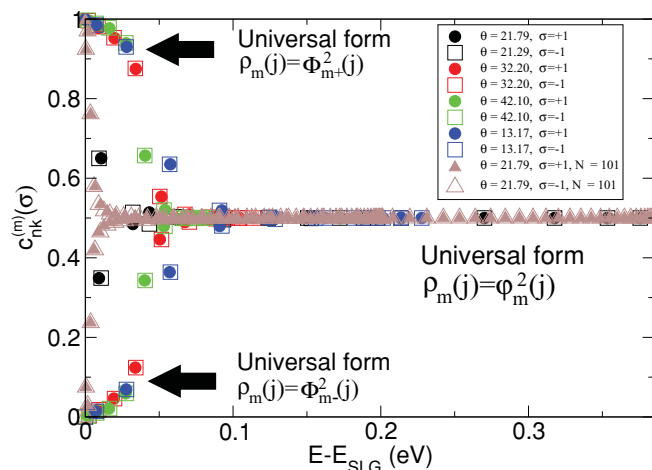

FIG. 3. (Color online) Numerical values for the coefficients $c_{n\mathbf{k}}^{(m)}(\sigma)$ in Eq. (5). Unless indicated all systems have 19 layers, with rotation angle displayed in caption.

leads to a low λ universal form for the density profile of either $\Phi_{m+}^2(j)$ or $\Phi_{m-}^2(j)$. The bifurcation in $\rho(1)$ follows as $\Phi_{m+}^2(j)$ has a large $\rho(1)$ and small $\rho(2)$ and vice versa for $\Phi_{m-}^2(j)$.

In experiment, of course, a certain amount of stacking disorder is always present, and thus a critical question is how well results for the fully ordered twist stack transfer to the case of realistic disordered graphene stacks. To this end we consider a pristine stack into which N_f faults are introduced at layers f_i. Such faulted layers are expected to couple standing wave states, and therefore once disorder is introduced the block diagonal structure of the Hamiltonian will be lost. Such off-diagonal matrix elements are readily evaluated giving

$$\left\langle \Phi_{m_1\sigma_1} \left| \delta H^{\alpha\beta} \right| \Phi_{m_2\sigma_2} \right\rangle = \sum_{\gamma=1}^{2} \sum_{i=1}^{N_f} 2\Phi_{m_1\sigma_1}(f_i)\Phi_{m_2\sigma_2}(f_i)$$
$$\times \delta t_{\gamma,f_i}^{\alpha\beta} \cos\left[\frac{(-m_\gamma + N_\perp + 1)}{2(N_\perp + 1)}\pi\right], \tag{6}$$

where $\delta H^{\alpha\beta}$ is the change in the (α, β) block of the Hamiltonian by the faulted layers, $\delta t_{1,f_i}^{\alpha\beta}$ the change in matrix elements that
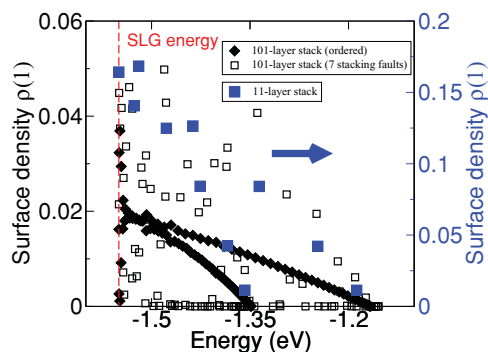

FIG. 4. (Color online) Weight of stack states at the first layer for a 101-layer ideal twist stack (filled symbols) and the same system with seven randomly distributed twist faults (open symbols). See text for details.

describe hopping *from* faulted layers to neighboring layers, and $\delta t_{2,f_i}^{\alpha\beta}$ the change in the matrix elements that describe hopping *to* neighboring layers from a faulted layer. Note that we here make no assumption on the nature or distribution of the faulted layers, other than that faulted layers are never nearest neighbors. From this expression we recognize that if $m_1 = m_2 = 0$ then the coupling is exactly zero and, more generally, that states having low m will be less coupled by disorder than those with high m. We thus see that of the $N_\perp$ Dirac cones, it is the "good graphene" low m cones that are least affected by stacking disorder.

For the purpose of numerical tight-binding calculations we now consider a specific type of rotation fault which, designating an ordered sequence of layers by $\ldots A_0 B_\theta A_0 B_\theta$, may be expressed as $\ldots A_0 B_0 A_0 B_\theta$. In Fig. 2(b) is shown the band structure of an 11-layer twist stack with such a rotation fault on the central layer. This amounts to the insertion of Bernal stacked AB sequences of layers, and so leads to the formation of defect bands close in nature to those of the Bernal stacked AB bilayer. The wave function associated with such a defect band is strongly localized on the faulted layer(s), shown both for the 11-layer case (lower inset) and for a 101-layer stack with seven twist faults (upper inset). These defect bands therefore have no impact on the quality of graphene found at the surface of the twist stack. Turning to an examination of the weight of the various Dirac cones at the twist stack surface we see from Fig. 4 that the introduction of disorder leads to a majority of states having zero weight at the surface. This may be understood as arising from standing wave states

resonating *between* stacking faults within the interior of the stack, which thus have no weight at the surface. On the other hand, the occurrence of a few states of enhanced weight at energies far from the SLG energy is due to states resonating between the surface itself and nearby stacking faults. As low m states are least affected by stacking disorder this reduction in surface weight is, as may clearly be seen in Fig. 3, dominated by the large m strongly coupled states. We thus find that that the results for the fully ordered twist stack are robust under moderate stacking disorder, and the surface is again dominated by low m "good graphene" states.

To conclude, we have examined the graphene twist stack, finding that this remarkable system mixes aspects of both low-dimensional physics with the three-dimensional physics of scalable epitaxial growth. Our analysis leads us to uncover a number of unexpected properties of the twist stack. In particular (i) the stack is heterogeneous: the quality of graphene at the surface and the interior of such a stack is markedly different, and (ii) states from bands closer topologically to the SLG cone are least affected by stacking disorder. These results raise the interesting possibility that by designing stack structures one may be able to manipulate and control the quality of graphene at the stack surface.

*phsss@tfkp.physik.uni-erlangen.de

[1] K. S. Novoselov, A. K. Geim, S. V. Morozov, D. Jiang, Y. Zhang, S. V. Dubonos, I. V. Grigorieva, and A. A. Firsov, Science **306**, 666 (2004).

[2] Walt A. de Heer, Clair Berger, Xiaosong Wu, Phillip N. First, Edward H. Conrad, Xuebin Li, Tianbo Li, Michael Sprinkle, Joanna Hass, Marcin L. Sadowski, Marek Potemski, and Gérard Martinez, Solid State Commun. **143**, 92 (2007).

[3] M. Sprinkle, D. Siegel, Y. Hu, J. Hicks, A. Tejeda, A. Taleb-Ibrahimi, P. Le Fèvre, F. Bertran, S. Vizzini, H. Enriquez, S. Chiang, P. Soukiassian, C. Berger, W. A. de Heer, A. Lanzara, and E. H. Conrad, Phys. Rev. Lett. **103**, 226803 (2009).

[4] M. Sprinkle, J. Hicks, A. Tejeda, A. Taleb Ibrahimi, P. Le Fèvre, F. Bertran, H. Tinkey, M. C. Clark, P. Soukiassian, D. Martinotti, J. Hass, W. A. de Heer, C. Berger, and E. H. Conrad, e-print arXiv:1001.3869 (to be published).

[5] Sylvain Latil, Vincent Meunier, and Luc Henrard, Phys. Rev. B **76**, 201402(R) (2007).

[6] J. Hass, F. Varchon, J. E. Millán-Otoya, M. Sprinkle, N. Sharma, W. A. de Heer, C. Berger, P. N. First, L. Magaud, and E. H. Conrad, Phys. Rev. Lett. **100**, 125504 (2008).

[7] J. M. B. Lopes dos Santos, N. M. R. Peres, and A. H. Castro Neto, Phys. Rev. Lett. **99**, 256802 (2007).

[8] S. Shallcross, S. Sharma, and O. A. Pankratov, Phys. Rev. Lett. **101**, 056803 (2008).

[9] S. Shallcross, S. Sharma, E. Kandelaki, and O. A. Pankratov, Phys. Rev. B **81**, 165105 (2010).

[10] E. J. Mele, Phys. Rev. B **81**, 161405 (2010).

[11] R. Bistritzer and A. H. MacDonald, Phys. Rev. B **81**, 245412 (2010).

[12] Mikito Koshino and Tsuneya Ando, Phys. Rev. B **76**, 085425 (2007).

[13] M. S. Tang, C. Z. Wang, C. T. Chan, and K. M. Ho, Phys. Rev. B **53**, 979 (1996).

[14] Close to the Dirac point due to the near degeneracy of all bands a different behavior is seen; however, this does not affect the arguments presented here.